Identification of material properties of composite sandwich panels under geometric uncertainty

Missoum, S; Lacaze, S.; Amabili, M.; Alijani, Farbod

Important note
To cite this publication, please use the final published version (if applicable).
Please check the document version above.

Identification of material properties of composite sandwich panels under geometric uncertainty

Samy Missoum [a],*, Sylvain Lacaze [a], Marco Amabili [b], Farbod Alijani [c]

[a] Aerospace and Mechanical Engineering, Department University of Arizona, Tucson, AZ, USA
[b] Department of Mechanical Engineering, McGill University, Montréal, Québec, Canada
[c] Department of Precision and Microsystems Engineering, TU Delft, The Netherlands

ABSTRACT

This study deals with the influence of manufacturing-induced geometric variability on the identification of material properties of composite sandwich panels. The objective of this article is twofold. First, this work aims to demonstrate the marked influence of geometric uncertainties on a foam core sandwich panel whose skin material properties need to be identified. Several identification cases are studied based on experimentally obtained natural frequencies and mode shapes. The second objective is to propose a numerical method for the identification process in the case where uncertainties can be treated as a random field (e.g., thickness distribution). The identification method is built around a classification-based technique referred to as "fidelity maps", which has the ability to simultaneously treat several responses to match without any assumption on their correlation. The approach uses a proper orthogonal decomposition for the extraction and the selection of the features of the random field considered as important for the identification. The identification method is demonstrated on a foam core sandwich panel whose thickness distribution is modeled as a random field.

© 2017 Elsevier Ltd. All rights reserved.

1. Introduction

The identification of material properties of composites can be made difficult due to numerous sources of uncertainty inherent to the manufacturing process. Uncertainties can take several forms such as inhomogeneous material distributions or uneven thickness distributions. It is now well established that uncertainties can have a significant effect on the behavior of composites [1–3] and must therefore be accounted for in any material property identification or model calibration process. Identification can be performed using static and/or dynamic experimental tests. In the dynamic case, which is of interest to this study, natural frequencies and mode shapes are typically used [4–8]. There exist several methods to perform identification such as the widely used least-square minimization of a residual [9,10], which quantifies the mismatch between prediction and experiments. Other techniques, such as maximum likelihood or Bayesian update [11,12], enable one to include uncertainties in the identification process. The inclusion of uncertainties is of prime importance since quantities such as natural frequencies and mode shapes might be highly sensitive to local variations in stiffness and mass distributions [1–3].

The identification process can be hampered by a number of factors. First, some uncertainties can be simply overlooked or poorly quantified (e.g., presence of a crack or local excess of glue) thus leading to wrong assessments. Second, several, potentially many, *correlated* responses might be needed to increase the identifiability of specific parameters [13,14]. Yet, existing methods do not properly account for several correlated responses. For instance, one might want to identify material properties based on several natural frequencies and mode shapes, which are correlated with each other. However, the widely used minimization of a residual based on several correlated responses can be shown to provide biased results when these responses are assumed independent, as it is usually done [13,15].

The first objective of this paper is to highlight the difficulties inherent to the identification process in the case of a manufactured foam core sandwich panel with unknown skin material properties [16,17]. Specifically, this study focuses on the influence of geometric variability on the quality of the modal data-based identification and corresponding finite element model calibration. This objective is carried out by comparing identification results, obtained by maximizing the agreement between model and experiments, for several scenarios such as a spatially constant thickness distribution or a measured thickness distribution over the panel.

---

* Corresponding author.
 E-mail address: smissoum@email.arizona.edu (S. Missoum).

In light of these results, the second objective is to provide a new methodology for the identification of material properties in the case where material or geometric properties form a random field. The proposed identification approach is based on notion of "fidelity maps" developed by the first two authors [13,14]. A fidelity map defines the region in the parameter space where a given level of agreement between computational results and measurements is achieved. The use of fidelity maps, which are approximated using a classification technique, such as a support vector machine (SVM) [18], has three major advantages. The first one is that it facilitates the propagation of uncertainty. In fact, the approach enables the identification of material properties using either maximum likelihood or Bayesian estimates [12,19]. The second advantage is the ability to handle many responses to match simultaneously, thus leading to more robust estimates. Finally, fidelity maps naturally capture the correlation structure between responses which is typically assumed or inexistent if other techniques are used. The fidelity map technique is extended to the case of random fields [20], which enable a more realistic representation of uncertainties (e.g., thickness distribution). The extension of the fidelity map approach to random fields is carried out by using the coefficients of a snapshot-based proper orthogonal decomposition (POD) of the field as random variables [20]. That is, the fidelity map is built in a space made of the parameters to identify as well as the random coefficients of the POD description. The approach is applied to a foam core sandwich panel whose thickness is modeled as a random field.

This article is structured as follows: Section I aims at demonstrating the influence of geometric uncertainties on the identification of material properties. The section also describes the foam core composite plate and the modal analysis experimental setup. Section II describes the fidelity map approach and its extension to random fields. Section III provides the results of the random field approach applied to the sandwich panel.

2. Influence of geometry on material identification

This section aims at providing insight into the difficulties inherent to the identification process due to geometric uncertainties. For this purpose, the identification of the skin properties of a foam core sandwich panel is performed using experimental modal data.

2.1. Foam core sandwich panel. Experimental setup

The panel, constituted of a foam core and two identical external skins, has a length $A = 900$ mm and a width $L = 460$ mm, and an average *total* thickness of $h = 3.3$ mm (Fig. 1a). The top and bottom skins are each constituted of a two layer Carbon/Epoxy (0/90) lay-up (where the 0 angle is the exterior layer, with fibers parallel to

the length direction). The thickness h_c of each Carbon/Epoxy layer is 0.17 mm. The plate has been manufactured at the Structures and Composite Materials laboratory at McGill University using a vacuum bag processing equipment. The plate has a DIAB Divinycell foam core with $E_{co} = 40$ MPa, $G_{co} = 9.5$ MPa, $\rho_{co} = 339.4$ kg/m^3, and an average core thickness h_{co} of 2.62 mm (Fig. 1b). Details on the experimental setup can be found in [17].

The modal analysis of the plate was performed using a plate under free edge conditions which was subjected to random excitation using a shaker. The free edge conditions were achieved by hanging the plate using low stiffness elastics. The measurements were performed using a non-contact laser scanning vibrometer by Polytec, Inc. A depiction of the experimental setup is provided in Fig. 2. The natural frequencies and damping ratios are provided in Table 1. The corresponding experimentally obtained modes are depicted in Fig. 3.

2.2. Basic identification through deterministic optimization

A first estimate of the skin material properties was carried out through deterministic optimization using the four first natural frequencies of the plate. The skin properties found are: $E_1 = 127$ GPa, $E_2 = 6.05$ GPa, $G_{12} = 5$ GPa, $G_{13} = G_{23} = 3.3$ GPa and $v = 0.35$ where the subscript 1 stands for the fiber direction, and 3 is the out-of-plane direction.

A linear Finite Element (FE) model of the sandwich panel was constructed using ANSYS shell 181 elements [21]. The shell 181 element is a multilayered shell element for thin to moderately thick shell structures and has the ability to account for transverse shear deformation (Mindlin-Reissner theory) [22–25]. While the stiffness matrix is numerically integrated, a consistent mass matrix with close form integration is used.

The numerical prediction for the first eight modes were obtained using the FE model. Table 2 provides the relative errors ε_i between the experimental *ith* natural frequencies and the FE predictions. The maximum relative error is provided in cases where 4 and 8 modes are compared. The nature and sequence of the FE mode shapes (Fig. 4) is similar to the experimental mode shapes depicted in 3. However, it is observed that a 13.25% error is obtained for the 6*th* mode. This difference can be partially explained by inspection of mode 6 obtained computationally and experimentally (see Figs. 3 and 4): although the computational mode 6 exhibits a perfect double symmetry, it is not the case for the experimental mode, which is only perfectly symmetrical with respect to the length-wise axis.

2.2.1. Uniform thickness assumption

In order to reduce the error, the total thickness h of the plate, considered uniform over the whole plate, is introduced as a
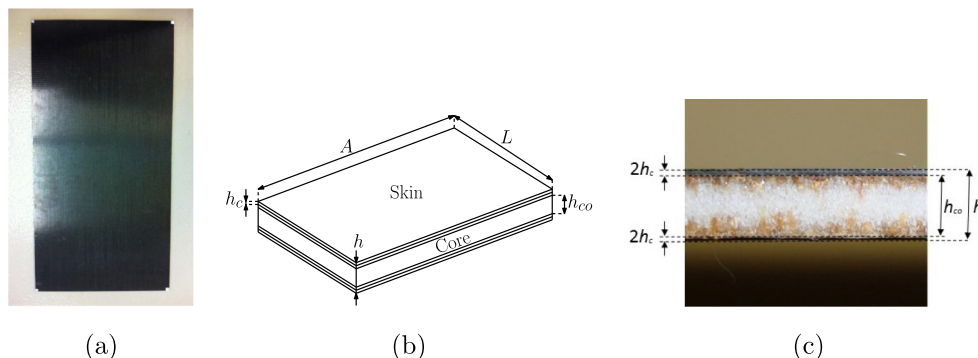

Fig. 1. (a) Top view of the foam core sandwich plate; (b) Schematic representation with dimension labeling. h_c is the thickness of one skin layer; (c) Detail showing the foam core and the external skins.
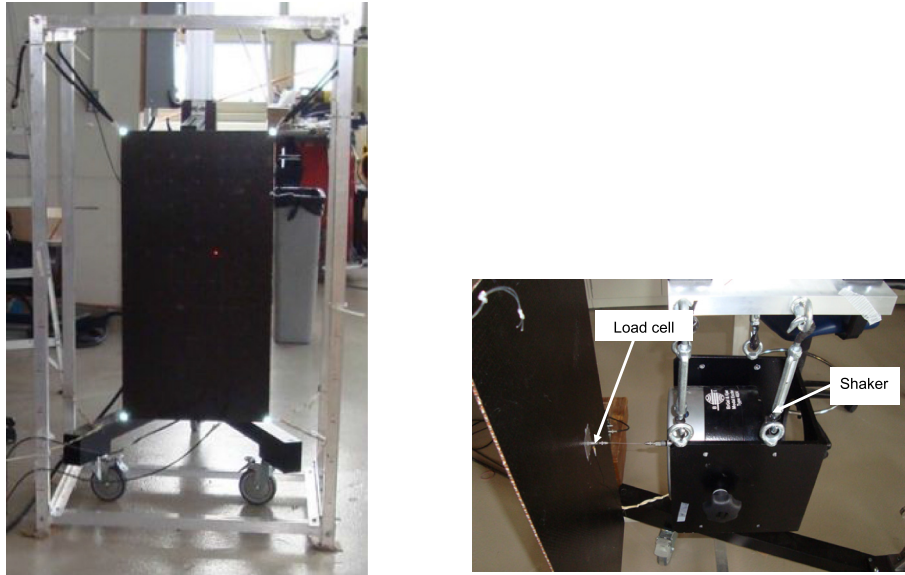
Fig. 2. Experimental setup. Front view (left); side view (right).

Table 1
Mode sequence, natural frequencies, and damping ratios obtained experimentally on the foam core sandwich panel. The letters A and S stand for "Antisymmetric" and "Symmetric" mode with respect to the two main axes of symmetry of the plate.

Mode Sequence	Natural Frequency (Hz)	Damping Ratio (%)
A,A-1	19.00	1.2
S,S-1	31.56	0.45
S,A-1	48.13	0.64
A,S-1	83.76	0.12
A,A-2	99.83	0.18
S,S-2	101.2	0.17
A,S-2	108.8	0.19
S,S-3	125.6	0.31

quantity to identify in addition to the two skin material properties E_1 and G_{12}. Other parameters are kept to the values provided in the previous section as they are either known or deemed not influential. The skin thickness is constant at 0.17 mm. For this identification, a pattern search algorithm [26] was used to find a set of parameters that minimizes the maximum absolute value of the relative error between the model and the experimental natural frequencies. For comparison, the optimization was successively based on the four and eight first natural frequencies (Table 3). Table 4 shows the estimated values for these three parameters for the two cases.

These results indicate that, using 8 natural frequencies, the error cannot be reduced below 6.87%. This could be attributed to the fact that the experimental setup was optimized for the first 4 modes. Note that the mode shapes are qualitatively similar to the ones in Fig. 4. In addition, the two optimizations converge to different optima for the cases where 4 modes and 8 modes are used. Therefore, the properties are *not clearly identifiable* and the results cannot be used with the present setting.

2.2.2. Actual thickness measurements

In an effort to further understand the discrepancies, spatial measurements of the thickness were performed along each side
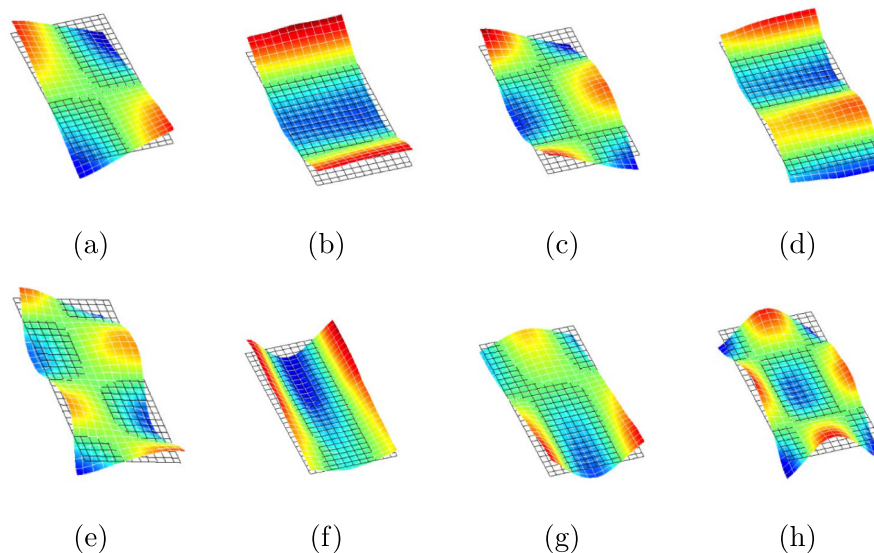

Fig. 3. First 8 mode shapes, experimentally identified. (a) 1st mode, A,A-1; (b) 2nd mode, S,S-1; (c) 3rd mode, S,A-1; (d) 4th mode, A,S-1; (e) 5th mode, A,A-2; (f) 6th mode, S,S-2; (g) 7th mode, A,S-2; (h) 8th mode, S,S-3.

Table 2
Experimental and FE-predicted natural frequencies. ε_i is the maximum relative error for the ith mode.

	Experimental (Hz)	FE (Hz)	ε_i (%)
λ_1	19.00	18.90	0.49
λ_2	31.56	31.74	0.58
λ_3	48.13	47.76	1.32
λ_4	83.76	82.67	1.29
λ_5	99.83	97.49	2.34
λ_6	101.24	114.65	13.25
λ_7	108.80	119.42	9.76
λ_8	125.66	135.98	8.21
		$\max(\varepsilon_1,\ldots,\varepsilon_4)$	1.32
		$\max(\varepsilon_1,\ldots,\varepsilon_8)$	13.25

Table 3
Identification of the (uniform) total thickness h, E_1 and G_{12} using 4 or 8 frequencies (λ_i).

		Use of 4 nat. freq.		Use of 8 nat. freq.	
	Experimental (Hz)	FE (Hz)	ε_i (%)	FE (Hz)	ε_i (%)
λ_1	19.00	18.76	1.28	18.89	0.56
λ_2	31.56	31.90	1.07	29.74	5.76
λ_3	48.13	48.75	1.28	47.58	1.14
λ_4	83.76	83.41	0.42	78.00	6.87
λ_5	99.83	98.14	1.69	93.82	6.02
λ_6	101.24	115.75	14.33	108.20	6.87
λ_7	108.80	120.54	10.79	113.34	4.17
λ_8	125.66	137.20	9.18	130.53	3.87
$\max(\varepsilon_1,\ldots,\varepsilon_4)$		1.28		6.87	
$\max(\varepsilon_1,\ldots,\varepsilon_8)$		14.33		6.87	

Table 4
Estimated material properties with a uniform plate thickness.

# of freq.	h (mm)	E_1 (GPa)	G_{12} (GPa)
4	3.6	101	4.88
8	3.3	110	6.07

of the plate. The observed variations are reported on Fig. 5. Based on these measurements, the thickness was assumed to be varying along the width of the plate and constant along its length. It can clearly be observed that there is a rather sharp change in the thickness about 0.2 m along the width, which might therefore substantially modify the bending stiffness of the plate locally. In order to apply this thickness distribution to the FE model, a polynomial was fitted to the measured data (Fig. 6). Analogous to the previous section with an overall constant thickness, a similar deterministic optimization was performed and the results are summarized in Table 5.

In contrast with the previous analysis, these results show that an error of 3.11% can be achieved and both optimizations converge to approximately the same optimum. These results are consistent and therefore are more likely to estimate the material properties of this specific plate. The mode shapes are qualitatively similar to the ones in Fig. 4. Note that the optimal values from this analysis (Table 6) are different from either solution of the first analysis. This clearly demonstrates the strong influence of the thickness distribution.

2.3. Sensitivity analysis

In order to assess the effect of material and geometric parameters on the natural frequencies and calibration error, a global sensitivity analysis is performed. This analysis is performed using Sobol indices [27], which quantify the fraction of the total variance of a response f (e.g., a natural frequency) due to a specific parameter x_i. Sobol indices are defined as follows:

First order indices, which provide the "main effect" of each parameter:

$$S_i = \frac{\mathbb{V}[\mathbb{E}(f|x_i)]}{\mathbb{V}[f]} \tag{1}$$

where $\mathbb{V}$ and $\mathbb{E}$ are the variance and expected value operators respectively.

Second order indices, which represent the variance contribution directly due to the coupling between the variables x_i and x_j:

$$S_{ij} = \frac{\mathbb{V}[\mathbb{E}(f|x_i,x_j)] - \mathbb{V}[\mathbb{E}(f|x_i)] - \mathbb{V}[\mathbb{E}(f|x_j)]}{\mathbb{V}[f]} \tag{2}$$

Finally, the total indices include first and second order effects:

$$S_i^T = \frac{\mathbb{E}[\mathbb{V}(f|x_{-i})]}{\mathbb{V}[f]} \tag{3}$$

where x_{-i} is the set of all the parameters expect x_i. Note that higher order coupling terms could also be calculated. For the study at hand, we will compare the total indices to measure the relative contribution of the parameters. From mechanics, the following parameters were chosen for the sensitivity analysis. The corresponding ranges are also provided:
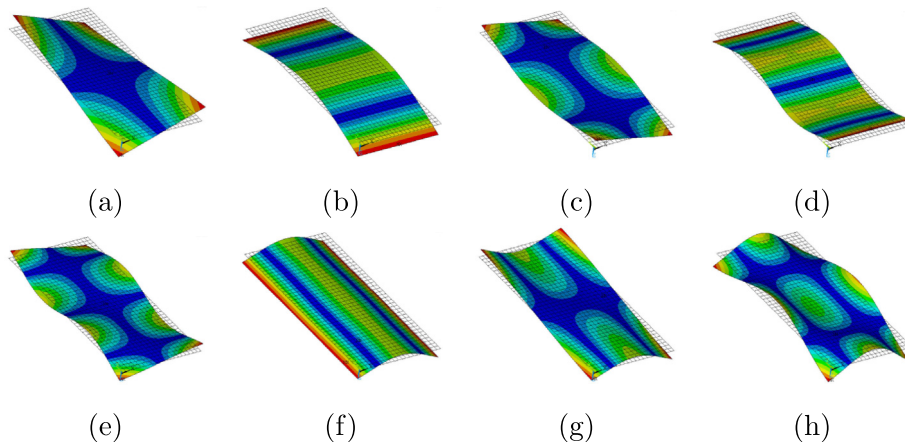

Fig. 4. First 8 mode shapes obtained computationally following the same sequence as experimental mode shapes. (a) 1st mode, A,A-1; (b) 2nd mode, S,S-1; (c) 3rd mode, S,A-1; (d) 4th mode, A,S-1; (e) 5th mode, A,A-2; (f) 6th mode, S,S-2; (g) 7th mode, A,S-2; (h) 8th mode, S,S-3.
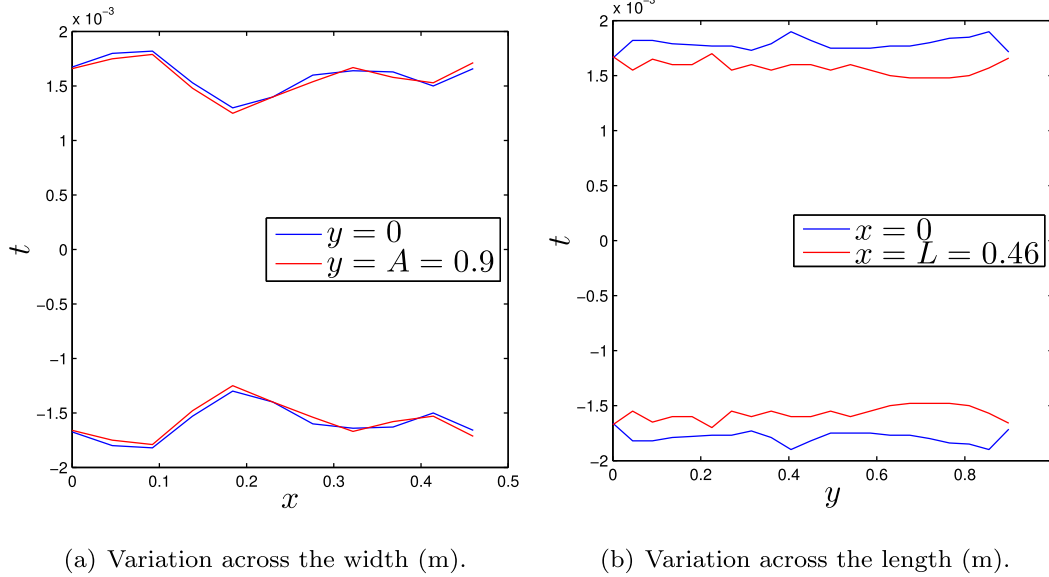
(a) Variation across the width (m).

(b) Variation across the length (m).

Fig. 5. Thickness measurement along the 4 sides of the plate. Measurements were performed using a digital caliper.
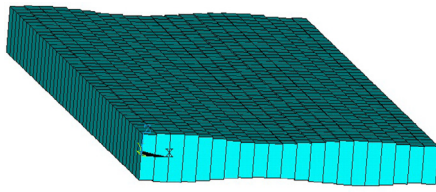

Fig. 6. Finite element model with varying thickness. The thickness distribution was measured experimentally and fitted with a polynomial.

Table 5
Calibration using fixed thickness distribution.

	Experimental (Hz)	Use of 4 nat. freq.		Use of 8 nat. freq.	
		FE (Hz)	ε_i (%)	FE (Hz)	ε_i (%)
λ_1	19.00	18.64	1.90	18.70	1.56
λ_2	31.56	31.91	1.11	31.25	0.99
λ_3	48.13	49.04	1.90	48.70	1.18
λ_4	83.76	82.68	1.29	81.15	3.11
λ_5	99.83	99.27	0.56	98.04	1.79
λ_6	101.24	106.45	5.14	104.39	3.11
λ_7	108.80	112.18	3.11	110.28	1.36
λ_8	125.66	131.01	4.26	129.39	2.97
$\max(\varepsilon_1,\ldots,\varepsilon_4)$	1.90			3.11	
$\max(\varepsilon_1,\ldots,\varepsilon_8)$	5.14			3.11	

Table 6
Estimated material properties (GPa) using fixed varying thickness.

λs	E_1 (GPa)	G_{12} (GPa)
4	136	6.63
8	131	6.69

- E_1: Young's modulus of the skin layers in the fiber direction. E_1 will substantially influence bending modes. $E_1 \in [100, 150]$ GPa.
- G_{12}: In plane shear modulus, which will torsional modes. $G_{12} \in [3.5, 7.5]$ GPa.
- h: Total thickness which substantially influences the bending stiffness. $h \in [3.0, 3.6]$ mm.

- h_c: Skin thickness (included in the total thickness). $h_c \in [0.17, 0.23]$ mm.
- ρ_{co}: foam core density. $\rho_{co} \in [300, 350]$ kg/m³.

While G_{12} and E_1 are to be identified, the three other parameters, h, h_c, and ρ_{co} can be measured. They are added to the sensitivity study to show their relative influence.

The calculation of accurate Sobol indices is based on sampling and is computationally intensive. In fact, a brute force sampling approach to obtain converged Sobol indices in a five dimensional space (i.e., with five parameters) with frequencies obtained using an FE code is not tractable. Instead, the frequencies and error measures are approximated using Kriging surrogates [28]. This considerably improves the computational efficiency.

The Sobol indices were computed using the CODES toolbox developed by the first author's group [29]. The relative importance of the total indices are presented in Fig. 7 for the eight first natural frequencies as well as the calibration error used in this article (i.e., $\max(\varepsilon_i)$). The material properties and the geometric parameters have a varying relative importance as a function of the mode. For instance, modes 1 and 3, which are torsional modes are largely influenced by the shear modulus G_{12}, while for a bending mode such as modes 2 and 4, E_1 will have a large influence. For all the modes, h and h_c are important, which is expected. Relatively to the other parameters, ρ_{co} as a minor importance except for mode 5. The results also show the similarity of sensitivities between mode 6 and the maximum error. This was expected as the maximum error was driven by mode 6. For the reader not familiar with Sobol indices, it is important to remember that the relative importance of the indices is a function of the parameter ranges chosen.

3. Identification method based on random fields and fidelity maps

This section proposes a general identification approach in the case where uncertainties form a random field as for the sandwich plate previously described. The approach is based on the notion of fidelity maps [13] and the extraction of a random field features through proper orthogonal decomposition (POD). Both techniques are presented in the subsequent sections.
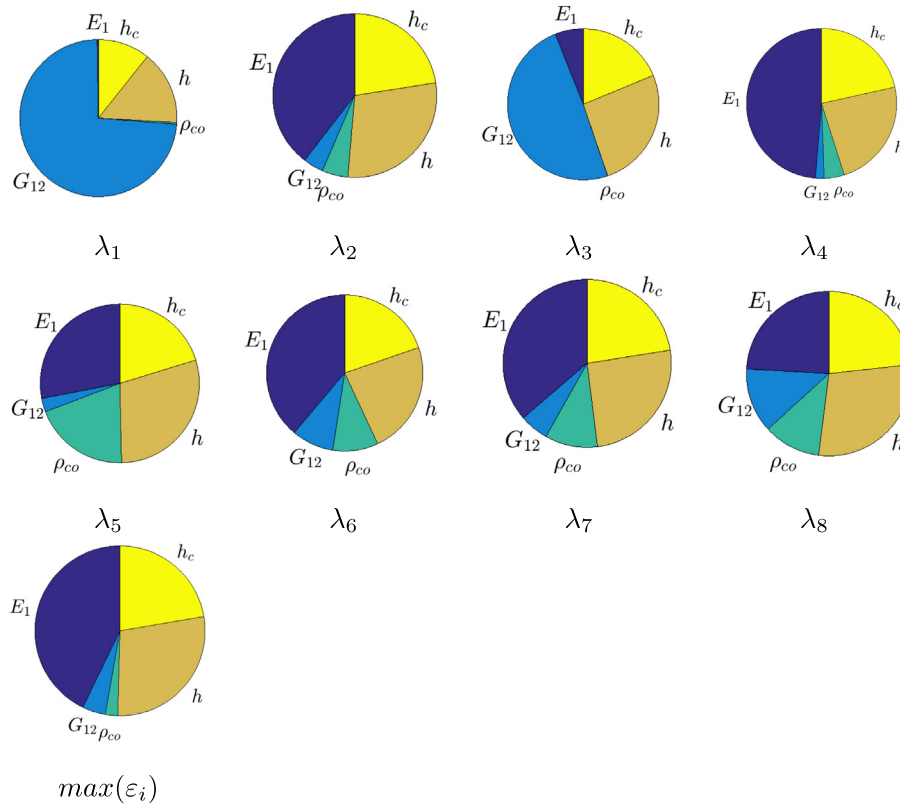
Fig. 7. Total sensivity indices relative importance for the first 8 natural frequencies λ_i as well as the maximum error $max(\varepsilon_i)$ used for identification.

3.1. Fidelity maps

Consider the responses **y** of a model and the corresponding experimental measurements $\mathbf{y}^{exp}$. The responses of the system are governed by two types of parameters: the first set are the parameters to estimate **p** (e.g., material property) while the second one, **A**, are the "aleatory" parameters which are not to be estimated but introduce uncertainty (e.g., loading or boundary conditions). A fidelity map is defined as the region of the parameter space corresponding to responses within a user-defined interval of the experimental data:

$$FM = \{(\mathbf{p}, \mathbf{a}) \mid r_i \leqslant \varepsilon_i, \ i = 1, \ldots, n\} \tag{4}$$

where n is the number is the number of responses (e.g., 8 frequencies in the case of the foam core plate) and

$$r_i = \left| \frac{y_i(\mathbf{p}, \mathbf{a}) - y_i^{exp}}{y_i^{exp}} \right|$$

This notion is illustrated in Fig. 8. It can be shown that the likelihood of any given $\mathbf{p}^*$ can be efficiently approximated (up to a constant) as the probability that $\mathbf{p}^*$ lies within the fidelity map, $\mathbb{P}[(\mathbf{p}^*, \mathbf{A}) \in FM]$ [13,30]. In general, the computation of such probability would lead to prohibitive computational cost. Therefore, the boundary of the fidelity map is approximated using a support vector machine (SVM) classifier. Probabilities can then be efficiently computed using Monte-Carlo simulations to provide maximum likelihood estimates of the parameters to identify.

3.2. Support vector machine (SVM)

An SVM defines the boundaries between samples of two distinct classes (e.g., acceptable and non-acceptable) [18,31–33]. Given Q training sample, an SVM classifier is expressed as:

$$s(\mathbf{x}) = b + \sum_{k=1}^{Q} \lambda^{(k)} l^{(k)} K(\mathbf{x}^{(k)}, \mathbf{x}) \tag{5}$$

where $\mathbf{x}^{(k)}$ is the kth training sample, $\lambda^{(k)}$ is the corresponding Lagrange multiplier, $l^{(k)}$ is the label (class) that can take values +1 or −1, K is a kernel function (e.g., Gaussian in this work) and b is the bias. The boundary is defined as $s(\mathbf{x}) = 0$ which splits the space into a positive and a negative region.

In order to build the fidelity map, an SVM is initially trained using a design of experiments (DOE). The class of each sample is defined based on the discrepancy between the model outputs and the experimental measurements. To be feasible (i.e., to belong to the fidelity map), a training sample must correspond to relative differences r_i between the model outputs y_i and the measurements y_i^{exp} less than a given threshold ε_i (i.e., the outputs lie within a "confidence region"). Therefore, the labels used to train the SVM are defined as:

$$l^{(k)} = \begin{cases} +1 & \text{if } r_i^{(k)} \leqslant \varepsilon_i, \ i = 1, \ldots, n \\ -1 & \text{otherwise} \end{cases}$$

where

$$r_i^{(k)} = \left| \frac{y_i^{(k)} - y_i^{exp}}{y_i^{exp}} \right|$$

3.3. Adaptive sampling for fidelity map refinement

In order to get an accurate approximation of the fidelity map boundary, an SVM, initially trained using a design of experiments, is sequentially refined. The adaptive sampling scheme used is based on a "max–min" sampling technique [34]. New samples
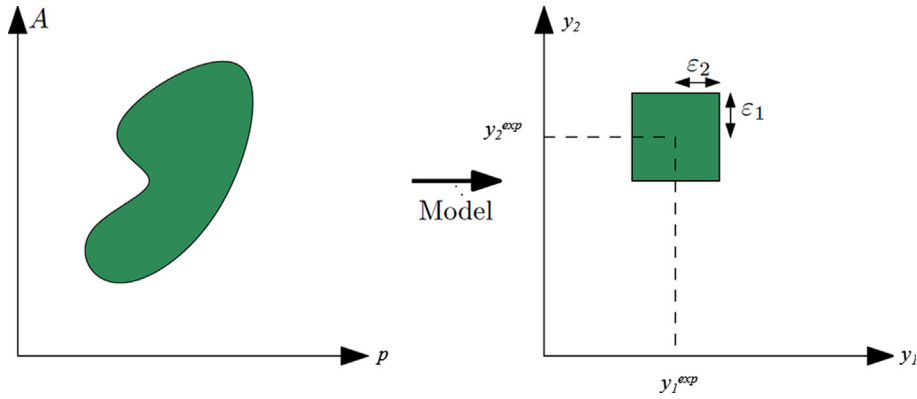
Fig. 8. Schematic representation of the fidelity map concept.

are defined as the points in space that maximize the minimum distance to existing samples (i.e., they are located in sparse regions) while lying on the SVM boundary:

$$\mathbf{x}_{mm} = \arg\max_{\mathbf{x}} \quad \min_{i} \|\mathbf{x} - \mathbf{x}_i\| \tag{6}$$

$$\text{s.t.} \quad s^{(k)}(\mathbf{x}) = 0 \tag{7}$$

$$\mathbf{l} \leqslant \mathbf{x} \leqslant \mathbf{u} \tag{8}$$

where $\mathbf{x}_i$ is the ith sample in the training set and $\mathbf{l}$ (resp. $\mathbf{u}$) are the lower (resp. upper) bounds of $\mathbf{x}$.

3.4. Identification with random fields. Proper orthogonal decomposition (POD)

A more general way to describe uncertainties is through a random field description. Consider a spatial random field defined as $\psi(\mathbf{x})$ (e.g., thickness distribution). In most applications, a random field can be discretized into a random vector (e.g., thickness at each element of a finite element model). A realization of the M component random vector (e.g., measurements of the thickness at M locations) is noted:

$$C = \begin{bmatrix} \psi(\mathbf{x}^{(1)}) \\ \vdots \\ \psi(\mathbf{x}^{(M)}) \end{bmatrix} = \begin{bmatrix} \psi_1 \\ \vdots \\ \psi_M \end{bmatrix} \tag{9}$$

In order to characterize such field, one typically relies on N realizations (e.g., repeated measurements over different plates manufactured using the same process) grouped as:

$$\boldsymbol{\Psi} = \begin{bmatrix} \psi_{11} & \cdots & \psi_{1N} \\ \vdots & \ddots & \vdots \\ \psi_{M1} & \cdots & \psi_{MN} \end{bmatrix} = \begin{bmatrix} R_1 \\ \vdots \\ R_M \end{bmatrix} = [C_1 \quad \cdots \quad C_N] \tag{10}$$

In order to drastically reduce the dimensionality of the problem, the main features of the random fields must be identified . This is achieved through proper orthogonal decomposition (POD).The general idea of POD is to analyze the covariance between the components of a random vector in order to extract the most important features of the field.

The first step of POD is to generate the mean random field:

$$\overline{C} = \begin{bmatrix} \overline{R}_1 \\ \vdots \\ \overline{R}_M \end{bmatrix} \tag{11}$$

where $\overline{R}_i = \frac{1}{N}\sum_{j=1}^{N}\psi_{ij}$. This allows one to generate a matrix with centered snapshots:

$$\boldsymbol{\Phi} = [C_1 - \overline{C} \quad \cdots \quad C_N - \overline{C}] = [\Phi_1 \quad \cdots \quad \Phi_N] \tag{12}$$

The covariance matrix is defined as:

$$\Sigma^2 = \frac{1}{N-1}\boldsymbol{\Phi}\boldsymbol{\Phi}^T \tag{13}$$

One can extract the eigenvalues λ_i and the eigenvectors V_i of Σ^2. As M is typically larger than N it is numerically more efficient to consider:

$$\Sigma^{2\prime} = \frac{1}{M-1}\boldsymbol{\Phi}^T\boldsymbol{\Phi} \tag{14}$$

Σ^2 and $\Sigma^{2\prime}$ have the same eigenvalues. Their eigenvectors are related as follows [20]:

$$V_i = \boldsymbol{\Phi}V_i' \tag{15}$$

Assuming that the eigenvectors are normalized to unity and the eigenvalues ordered in decreasing order, the random field can be approximated as follows:

$$C_i \approx \overline{C} + \sum_{j=1}^{t}\alpha_{ij}V_j \qquad \text{with} \qquad \alpha_{ij} = \Phi_i^T V_j \tag{16}$$

where t is the number of eigenvalues considered. The eigenvalues represent the importance of a feature in the description of the random field. t is typically calculated so that the selected features provide the largest contribution to the field. This is done by computing the relative weight of each eigenvalue:

$$\rho_i = \frac{\lambda_i}{\sum_{j=1}^{N}\lambda_j} \tag{17}$$

t is chosen as the smallest number of features so that $\sum_{i=1}^{t}\rho_i \geqslant \gamma$. Typical values for γ are 0.95 or 0.99 which can be reached in some cases even for a rather small number of selected
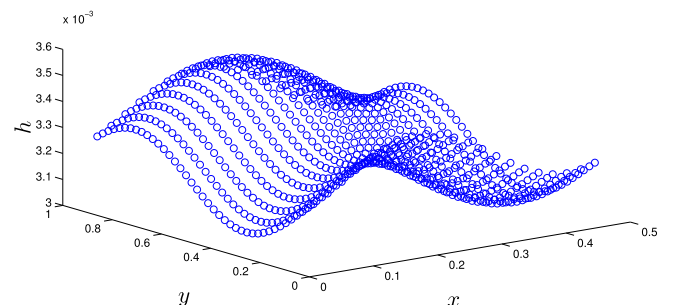

Fig. 9. An instance of the simulated random field representing the thickness distribution.

features (i.e., small t). It is important to realize that for a given j, α_{ij} are N ($i = [1, \ldots, N]$) independent realizations of a unique random variable α_j such that:

$$C \approx \overline{C} + \sum_{j=1}^{t} \alpha_j V_j \quad (18)$$

In this study, the coefficients α_j are considered as aleatory variables which are added to the dimensions of the space where the fidelity map is constructed. This way, the identification process will now account for random spatial variability.

4. Random field-based identification. Application to the foam core sandwich panel

The previous identification provided accurate estimates of the material properties of a specific plate. However, if another plate were to be produced from the same manufacturing process, would these estimates still be valid? A more robust approach consists of treating the thickness as a random field and to estimate the material properties under uncertainties. At this time, only one set of measurements of the thickness is available to the authors. Therefore, in order to demonstrate the methodology, a random field is assumed.

The thickness, defined as a random field, is defined as (in mm):

$$h(x, y) = 3.3 + \beta_1 \sin\left(2\pi \frac{x}{L} + \beta_3\right) + \beta_2 \sin\left(2\pi \frac{y}{A} + \beta_4\right) \quad (19)$$

where β_i are random coefficients with the following distributions:

$$\beta_1, \beta_2 \sim \mathcal{U}(0, 0.15)$$

$$\beta_3, \beta_4 \sim \mathcal{N}(0, 1)$$

Based on this random field description of the thickness, we wish to identify the skin properties E_1 and G_{12}. The finite element model uses $M = 840$ elements over which the random field is discretized as a random vector. A realization of this field is depicted on Fig. 9. A matrix of $N = 200$ snapshots of the thickness distribution was created using Eq. 19. Using POD, $t = 4$ important features were isolated ($\gamma = 0.99$). Fig. 10 shows the histograms and the fitted distributions using kernel density estimation [35] for the four relevant α_is.

In the absence of actual experimental values for the identification, a set of artificial experimental measurements was created using $E_1^{act} = 130.5$ GPa, $G_{12}^{act} = 5$ GPa and $\boldsymbol{\alpha} = [1, 2, 1, 1] \times 10^{-3}$. An SVM-based fidelity map was constructed for different thresholds ε (5%, 2%, and 1%) in the six dimensional space ($E_1, G_{12}, \alpha_1, \alpha_2, \alpha_3, \alpha_4$). For simplicity, the same threshold was used
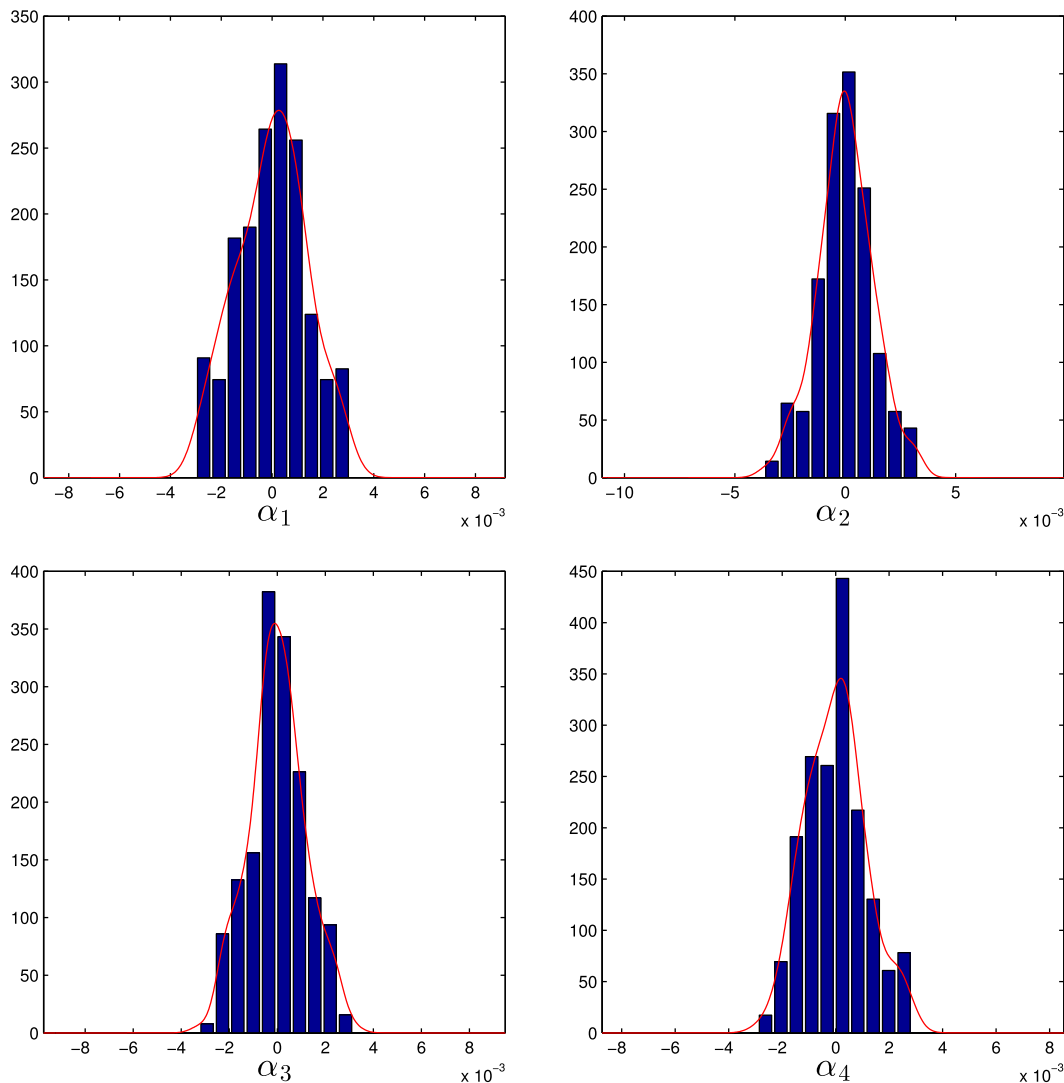

Fig. 10. Histogram and fitted distribution of the α_i parameters. Four α_is were selected using a POD of the random field with 200 snapshots.

(a) $\varepsilon = 5\%$ (b) $\varepsilon = 1\%$
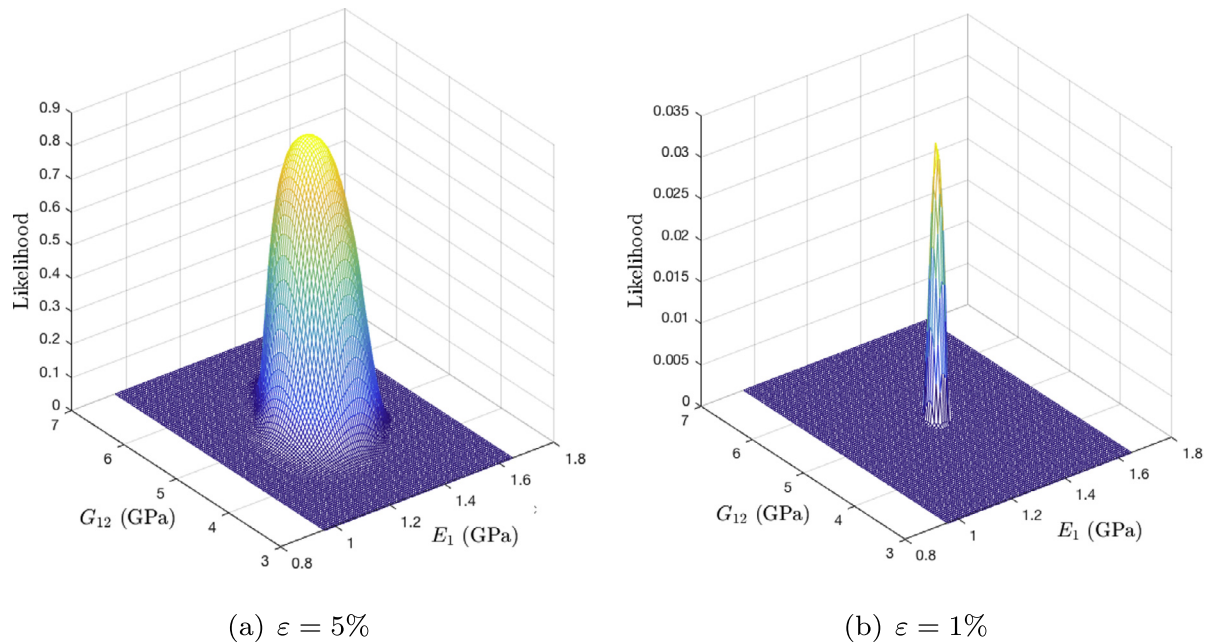
Fig. 11. Approximated likelihood using two fidelity maps for two values of ε.

Table 7
Random field analysis. Identified value of the skin properties E_1^{est} and G_{12}^{est} based on fidelity maps constructed with actual parameter values $E_1^{act} = 130.5$ GPa and $G_{12}^{act} = 5$ GPa.

ε (%)	DOE size	# of adap. samp.	E_1^{est} ($error_1$[a])	G_{12}^{est} ($error_2$[b])
5	60	100	132.94 GPa (1.87)	5.22 GPa (4.45)
2	60	200	131.55 GPa (0.80)	5.02 GPa (0.40)
1	60	300	130.85 GPa (0.27)	5.06 GPa (1.21)

[a] $error_1 = 100 \times \frac{|E_1^{act} - E_1^{est}|}{E_1^{act}}$

[b] $error_2 = 100 \times \frac{|G_{12}^{act} - G_{12}^{est}|}{G_{12}^{act}}$

for all 8 frequencies. For each threshold, an initial DOE of 60 points was used and the SVM was sequentially refined using 100, 200 and 300 adaptive samples. The lower ε is, the more adaptive samples are required to reach convergence.

Using the constructed fidelity maps, the likelihoods were approximated as shown on Fig. 11. Once again, it is important to realize that the fidelity maps are defined in a six dimensional space and that while E_1 and G_{12} are to be identified, the $\alpha_i s$ are treated as aleatory variables. The results are summarized in Table 7. They clearly demonstrate that as ε reduces, the estimation error reduces. For instance, in the case where $\varepsilon = 1\%$, the estimation error for the Young's modulus is below 0.3%.

5. Conclusion

In this article, the difficulties inherent to the identification of material properties of a sandwich panel were demonstrated. It was observed that geometric variability such as the thickness distribution might have a very large effect on the identification results. It was shown that assuming a constant thickness could lead to poor results as even small spatial variation of the thickness can significantly influence the modal properties. To improve the identification process under uncertainty, a methodology based on fidelity maps and a random field description was introduced for the modal data-based identification of the sandwich panel.

Subsequent steps of this research will include an actual characterization of the random field using experimental data from several sandwich panels. In addition, other sources of uncertainties, such as local or distributed changes in mass due to the presence of glue, will be investigated. The identification will also be extended to the case of nonlinear behavior, including large deformations.

References

[1] Chandrashekhar M, Ganguli R. Damage assessment of composite plate structures with material and measurement uncertainty. Mech. Syst. Sig. Process. 2016;75:75–93. http://dx.doi.org/10.1016/j.ymssp.2015.12.021.
[2] Onkar A, Upadhyay C, Yadav D. Stochastic finite element buckling analysis of laminated plates with circular cutout under uniaxial compression. J. Appl. Mech. Trans. ASME 2007;74(4):798–809. http://dx.doi.org/10.1115/1.2711230. cited By 23..
[3] Sepahvand K, Scheffler M, Marburg S. Uncertainty quantification in natural frequencies and radiated acoustic power of composite plates: analytical and experimental investigation. Appl. Acoust. 2015;87:23–9. http://dx.doi.org/10.1016/j.apacoust.2014.06.008.
[4] Marwala T. Finite Element Model Updating Using Computational Intelligence Techniques: Applications to Structural Dynamics. Springer; 2010.
[5] Mottershead J, Friswell M. Model updating in structural dynamics: a survey. J. Sound Vib. 1993;167(2):347–75. http://dx.doi.org/10.1006/jsvi.1993.1340.
[6] Tam JH, Ong ZC, Ismail Z, Ang BC, Khoo SY. Identification of material properties of composite materials using nondestructive vibrational evaluation approaches: A review. Mech. Adv. Mater. Struct. 2016:1–16.
[7] Deobald LR, Gibson RF. Determination of elastic constants of orthotropic plates by a modal analysis/rayleigh-ritz technique. J. Sound Vib. 1988;124(2):269–83.
[8] Ragauskas P, Belevičius R. Identification of material properties of composite materials. Aviation 2009;13(4):109–15.
[9] A. Bjorck, Numerical methods for least squares problems, no. 51, Society for Industrial Mathematics, 1996.
[10] Kariya T, Kurata H. Generalized Least Squares, Vol. 560. John Wiley & Sons Inc; 2004.

[11] K.-V. Yuen, Bayesian Methods for Structural Dynamics and Civil Engineering, 2010, cited By 170. doi: http://dx.doi.org/10.1002/9780470824566.
[12] Casella G, Berger RL. Statistical Inference, Vol. 70. CA: Duxbury Press Belmont; 1990.
[13] Lacaze S, Missoum S. Parameter estimation with correlated outputs using fidelity maps. Probab. Eng. Mech. 2014;38:13–21. http://dx.doi.org/10.1016/j. probengmech.2014.08.002.
[14] Lacaze S, Missoum S. Fidelity maps for model update under uncertainty: Application to a piano soundboard. American Institute of Aeronautics and Astronautics; 2012.
[15] Gogu C, Haftka R, Le Riche R, Molimard J, Vautrin A, et al. Introduction to the bayesian approach applied to elastic constants identification. AIAA J. 2010;48 (5):893–903. http://dx.doi.org/10.2514/1.40922.
[16] Alijani F, Amabili M. Nonlinear vibrations of laminated and sandwich rectangular plates with free edges. part 1: theory and numerical simulations. Compos. Struct. 2013;105:422–36.
[17] Alijani F, Amabili M, Ferrari G, Alessandro VD. Nonlinear vibrations of laminated and sandwich rectangular plates with free edges. part 2: experiments & comparisons. Compos. Struct. 2013;105:437–45.
[18] Vapnik V. The Nature of Statistical Learning Theory. Springer Verlag; 2000.
[19] Lai T, Ip K. Parameter estimation of orthotropic plates by bayesian sensitivity analysis. Compos. Struct. 1996;34(1):29–42.
[20] Basudhar A, Missoum S. A sampling-based approach for probabilistic design with random fields. Comput. Methods Appl. Mech. Eng. 2009;198 (47):3647–55.
[21] ANSYS Manual-Mechanical APDL/Theory [13] reference/15.7. 11.4.
[22] Carrera E. Theories and finite elements for multilayered, anisotropic, composite plates and shells. Arch. Comput. Methods Eng. 2002;9(2):87–140. http://dx.doi.org/10.1007/BF02736649.
[23] Reddy JN. Mechanics of Laminated Composite Plates and Shells: Theory and Analysis. CRC Press; 2004.
[24] Amabili M. Nonlinear Vibrations and Stability of Shells and Plates. Cambridge University Press; 2008.
[25] Bathe K-J, Dvorkin EN. A formulation of general shell elements the use of mixed interpolation of tensorial components. Int. J. Numer. Meth. Eng. 1986;22(3):697–722.
[26] Lewis RM, Torczon V. Pattern search algorithms for bound constrained minimization. SIAM J. Optim. 1999;9(4):1082–99.
[27] Sobol' IM, Kucherenko S. Derivative based global sensitivity measures and their link with global sensitivity indices. Math, Comput. Simul. 2009;79 (10):3009–17. http://dx.doi.org/10.1016/j.matcom.2009.01.023. arXiv:1605.07830.
[28] Stein ML. Interpolation of Spatial Data: Some Theory for Kriging. Springer Science & Business Media; 2012.
[29] S. Lacaze, S. Missoum, CODES: A Toolbox for Computational Design V. 1. URL: www.codes.arizona.edu/toolbox.
[30] S. Lacaze, S. Missoum, Bayesian calibration using fidelity maps, in: 11th International Conference on Structural Safety & Reliability, 2013.
[31] S. Gunn, Support vector machines for classification and regression, ISIS technical report 14.
[32] Schölkopf B, Smola A. Learning with Kernels: Support Vector Machines, Regularization, Optimization, and Beyond. The MIT Press; 2002.
[33] Christianini N, Taylor S. An introduction to support vector machines and other kernel-based learning methods. Cambridge University Press; 2000.
[34] Basudhar A, Missoum S. An improved adaptive sampling scheme for the construction of explicit boundaries. Struct. Multidiscipl. Optim. 2010;42 (4):517–29. http://dx.doi.org/10.1007/s00158-010-0511-0.
[35] Bowman A, Azzalini A. Applied Smoothing Techniques for Data Analysis: The Kernel Approach with S-Plus Illustrations, Vol. 18. USA: Oxford University Press; 1997.